

Electroadsorption of different valence ions on an HNO₃-modified activated carbon/nickel foam electrode

Quan Yuan¹, Haihong Li^{1,*}, Haojie Liu²

¹ School of Environmental and Chemical Engineering, Xi'an Polytechnic University, Xian, 710048, P. R. China

² Power China Beijing Engineering Corporation LTD, Beijing, 100024, P. R. China

*E-mail: 1624116019@qq.com

Received: 20 June 2022/ Accepted: 28 July 2022/ Published: 10 October 2022

In this study, nitric acid-modified activated carbon was used as the raw material to prepare electrodes for electroadsorption, and the adsorption and removal characteristics of eight common metal salt ions were investigated. The properties of the materials before and after modification were characterized and analyzed by a scanning electron microscope, a specific surface area and porosity analyzer, an infrared spectrometer, an electrochemical workstation, etc. The results show that the modified activated carbon has a better pore structure and more oxygen-containing functional groups than before, which results in better performance of the prepared electrode. According to the results of the desalination experiment, the prepared electrodes have a higher removal efficiency and a lower removal rate for higher valence ions, while for the same valence ions, a smaller radius of hydrated ions corresponds to higher removal efficiency and removal rate. The process of ions moving from the solution to the electrode surface and subsequently to the inside of the pore of the active material is mainly a physical adsorption process, but there is also weak chemisorption. This study provides a reference for the practical application of electrode desalination.

Keywords: Activated carbon, Electrode preparation, Electroadsorption, Adsorption kinetics

1. INTRODUCTION

In recent years, high-salt wastewater has been increasingly produced in many ways. In this study, a highly efficient, low-consumption and environmentally friendly desalination technology, called capacitive deionization (CDI), was used as the guide, and the desalination characteristics of electroadsorption demineralization technology were studied. Based on the principle of a double electric layer, voltage is applied to the electrodes to generate an electrostatic field between the electrode plates. Under the electrostatic field, the positive and negative ions in the solution migrate to two electrode plates

and are adsorbed in the double electric layer formed by the porous material on the electrode surface and liquid phase to remove salt[1].

The core of the electrosorption device is the electrode material, and research on electrode materials has gradually become the focus of electrosorption technology in recent years. Activated carbon electrodes are often used as electrode materials because of their large specific surface area, porous structure, stable chemical properties and renewability[2-3]. The adsorption performance of activated carbon is often improved by modifying and expanding the pores or by loading many oxygen-containing groups[4]. Alencherry T et al.[5] prepared an electrode by impregnating activated carbon with silver and adding carbon nanotubes. They found that the removal rate of salt ions increased from 42% to 67%, and the electric adsorption capacity of the electrode increased from 2 mg/g to 5.3 mg/g, since the conductivity and hydrophilicity of the electrode were enhanced through modification, which improved the adsorption capacity of the electrode for salt ions. Zou et al.[6] prepared an electrode by adding more active groups on the surface of an activated carbon material modified by a KOH solution. They found that the electric adsorption capacity increased by 5% compared to the original, probably because these groups helped improve the adsorption performance of the electrode. Chen et al.[7] studied the electrical adsorption performance of activated carbon electrodes in a salt solution with different potentials and concentrations. They found that with increasing bias potential and electrolyte concentration, the electrical adsorption capacity and adsorption rate increased. In addition, the electrical adsorption process of NaCl followed the Langmuir adsorption isotherm and quasi-first-order adsorption kinetics equation. The increase in adsorption rate was mainly due to the increase in electrostatic force and decrease in ion adsorption resistance.

There are few reports on the electrosorption characteristics of activated carbon electrodes for different salt ions. In this study, activated carbon was modified using HNO₃[8], and nickel foam was used as the current collector to prepare electrodes. A simulated desalting experiment on salt solutions with different ions and concentrations was performed to explore the characteristics of electric adsorption from the perspective of adsorption kinetics, which is of great importance for the practical application of electroadsorption technology.

2. EXPERIMENT

2.1 Materials and reagents

The activated carbon in this experiment was homemade biomass activated carbon from the laboratory (cotton straw as raw material; ZnCl₂/AlCl₃ activator; impregnation ratio of 9:1; activation temperature of 640°C).

Chemical reagent: nitric acid (A. R), superconducting electric carbon black (A. R), N,N-dimethylacetamide (A. R), polyvinylidene fluoride (A. R), sodium chloride (A. R), potassium chloride (A. R), manganese chloride (A. R), calcium chloride (A. R), magnesium chloride (A. R), zinc chloride (A. R), ferric chloride (A. R) and aluminum chloride (A. R).

The experimental instruments in this study were: a scanning electron microscope (Flex SEM 1000, Hitachi of Japan), a specific surface area and porosity analyzer (ASSAP 2020, Micromeritics Corporation, USA), a Raman spectrometer (Horibajy, France), an intelligent FTIR spectrometer (Nicolet 5700, Nicolet Corporation, USA), X-ray photoelectron spectroscopy (K-Alpha, Thermo Corporation, USA), an electrochemical workstation (CHI760D, Shanghai Huachen Instrument Co) and a digital conductivity meter (DDS-11A, Shanghai Magnetics Instruments Co).

2.2 Experimental content

(1) Preparation of modified activated carbon materials (HNO₃-AC)

In this study, activated carbon was modified by nitric acid oxidation. Two grams of activated carbon was immersed in 44% HNO₃ for 4 h and subsequently cleaned with deionized water until its conductivity was less than 10 (μS/cm). After drying and grinding, modified activated carbon was obtained. It was denoted by HNO₃-AC.

(2) Preparation of modified activated carbon electrodes (HNO₃-AC/Ni electrodes)

First, 0.15 g of PVDF was completely dissolved in 10 ml of N,N-dimethylacetamide under ultrasonic conditions; then, 0.9 g of HNO₃-AC and 0.11 g of superconducting carbon black were added. The mixture was stirred well on a magnetic stirrer. At a constant temperature of 80 °C, the mixture was evenly coated on the nickel foam current collector by the steam coating method and dried to obtain the HNO₃-AC/Ni electrode[9]. The electrodes were cut into 3 cm×1 cm pieces for testing.

(3) Electrochemical Testing

The cyclic voltammetry (CV) test (scanning rate 0.05 V/s, electrolyte 1 mol/L NaCl solution) and AC impedance test (frequency 0.01 ~ 100,000 Hz) of the electrode were measured using an electrochemical workstation (TYPE CHI760D).

(4) Preparation and standard curve drawing of ionic solutions with different valence states

To prepare metal salt solutions containing K⁺, Na⁺, Ca²⁺, Zn²⁺, Mg²⁺, Mn²⁺, Al³⁺ and Fe³⁺ ions, chloride metal salts were uniformly used to avoid the possible influence of metal salt compounds with different anions. KCl, NaCl, CaCl₂, ZnCl₂, MgCl₂, MnCl₂, AlCl₃ and FeCl₃ were used to prepare salt solutions at 20 mmol/L, 40 mmol/L, 60 mmol/L, 80 mmol/L and 100 mmol/L concentrations, respectively. The conductivity of different ions and salt solutions with different concentrations was measured at room temperature using a digital conductivity meter, and the conductivity (σ)-concentration (c) standard curve was plotted for each ion.

(5) Electroadsorption experiments

Two electrodes were connected in series to a DC regulated power supply. The working voltage was set to 1.5 V, the spacing between the plates was 0.5 cm, the initial concentration of the solution was 100 mmol/L, and the electroadsorption process lasted 120 min. The conductivity of the static solution was instantly measured with a digital conductivity meter and recorded every 10 min.

According to the conductivity (σ)-concentration (c) relation equation of the corresponding ions, the ion concentration in the solution at a certain time can be obtained. Then, the ion adsorption capacity Q at this time can be calculated using Equations (1) and (2):

$$n = (C_0 - C_t) v \quad (1)$$

where n is the amount of adsorbed ionic material (mmol), C_0 is the initial solution concentration (mmol/L), C_t is the concentration of the solution at time T (mmol/L), which can be calculated from the σ - c relation equation, and V is the solution volume (L).

$$Q = nM \quad (2)$$

where Q is the electric adsorption amount (mg), and M is the number of ionic substances (mg/mmol).

The ion removal rate can be calculated from Equation (3):

$$r = [(C_0 - C_t) / C_0] \times 100\% \quad (3)$$

where r is the ion removal rate.

2.3 Analysis of the adsorption kinetic model

(1) Kinetics of the quasi-first-order adsorption reaction

Theoretically, it is assumed that the adsorption process is dominated by physical adsorption, and the adsorption rate is determined by a single diffusion factor. The basic rate equation is as follows:

$$\ln(q_e - q_t) = \ln(q_e) - k_1 t \quad (4)$$

where q_e is the saturated adsorption at equilibrium (mg/g), q_t is the adsorption capacity at time T (mg/g), and k_1 is the rate constant of quasi-first-order adsorption in the adsorption process (min^{-1}).

(2) Quasi-secondary adsorption kinetics

Theoretically, it is assumed that the adsorption process is mainly chemical adsorption, where there may be interactions between adsorbent and solute, and many factors affect the adsorption rate. The basic rate equation is as follows:

$$\frac{t}{q_t} = \frac{t}{q_e} + \frac{1}{k_2 q_e^2} \quad (5)$$

where k_2 is the rate constant of quasi-secondary adsorption in this adsorption process (min^{-1}).

(3) Intraparticle diffusion model

Intraparticle diffusion is usually used to reflect the diffusion process inside particles, which is different from the diffusion process on the surface of particles and in liquid films. The basic rate equation is as follows:

$$q_t = k_n t^{1/2} \quad (6)$$

where k_n is the rate constant of intraparticle diffusion during the adsorption process (min^{-1}).

3. RESULTS AND DISCUSSION

3.1 Scanning electron micrograph analysis

Figure 1 shows the surface morphology of the original AC and modified HNO_3 -AC under a scanning electron microscope.

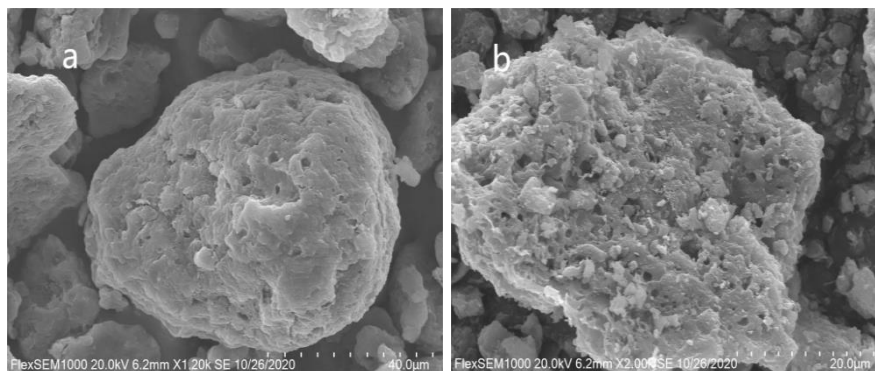


Figure 1. SEM images: (a) AC; (b) HNO₃-AC

Fig. 1 (a) shows that the pore structure of unmodified AC exhibits an undeveloped pore structure, and there is a small amount of pore structure. Fig. 1 (b) shows that the pore structure of HNO₃-modified AC is well developed and has more pore channels after oxidative expansion. This is beneficial to the transfer and diffusion of ions and the formation of a double electric layer by contacting the activated carbon with the liquid surface during the electrosorption process. Liu et al.[10] found that the structure of the activated carbon electrode material changed after the electrochemical activation, which made it have more pores and increased the contact area between liquid and active material, which improved the electric adsorption capacity of the electrode.

Field emission scanning electron microscopy images of the original nickel foam sample and HNO₃-AC/Ni electrode are shown in Figure 2.

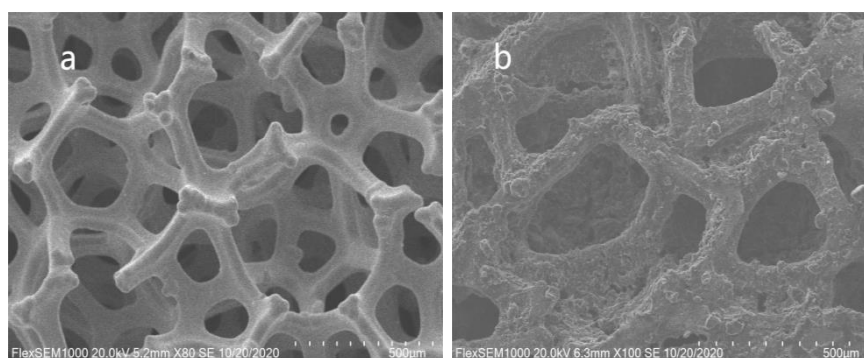


Figure 2. SEM images: (a) original nickel foam; (b) HNO₃-AC/Ni electrode

Fig. 2 (a) shows that the three-dimensional skeleton structure of nickel foam is well developed. Fig. 2 (b) shows the electrodes prepared by HNO₃-modified activated carbon. The figure shows that the HNO₃-AC material is uniformly wrapped around the Ni skeleton and maintains a complete three-dimensional skeletal structure. The nickel foam current collector plays the role of support and current transmission, which increases the contact area between the active material and the solution and the capacity of the double electric layer. Jiang et al.[11] optimized the pore size structure of an activated carbon electrode material using phosphoric acid, which achieved an electrosorption load of 19.28 mg/L.

3.2 Specific surface area and porosity analyzer

Figure 3 shows the isothermal curve of AC adsorption and desorption by calculating the specific surface area, pore diameter and pore volume before and after the AC modification through the nitrogen adsorption and desorption test.

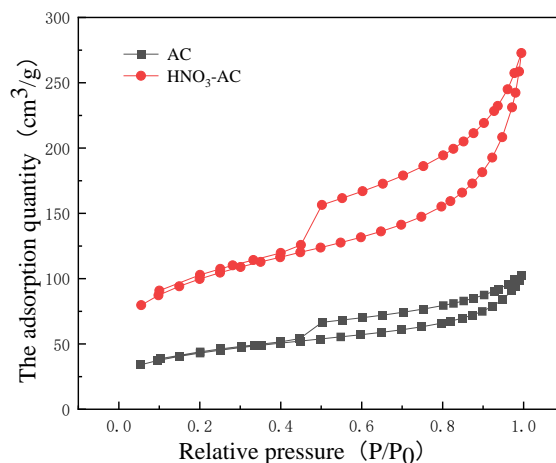


Figure 3. Nitrogen adsorption and desorption isotherms

HNO₃-AC has a much larger adsorption capacity than AC, and the adsorption and desorption isotherms of both materials belong to class IV[12]. When the relative pressure is low, the adsorption isotherms of the two materials slowly increase, which indicates that there is no micropore filling phenomenon, and there are very few micropores in the materials. When the relative pressure gradually increases, the adsorption capacity gradually increases. At a relative pressure from 0.5 to 1.0, the adsorption capacity of the material significantly increases, which ultimately results in a greatly increased adsorption capacity. Simultaneously, the desorbed branch always has a higher adsorption capacity than the adsorbed branch, and an H4-type hysteresis loop appears due to the mesopore capillary condensation. This is a common phenomenon in activated carbon materials, which indicates that the mesopores mainly play a role in adsorption at this time[13].

To further analyze the pore structure changes of AC before and after modification, the pore structure parameters and pore size distribution of the two samples were compared, as shown in Table 1 and Fig. 4. After the HNO₃ modification, the specific surface area, total pore volume and average pore size increased from 148.17 m²/g, 0.16 cm³/g and 4.3 nm to 341.38 m²/g, 0.42 cm³/g and 4.9 nm, respectively, because the oxidation of HNO₃ can produce a pore structure and expand micropores into mesopores or macropores. This change is conducive to the increase in adsorption capacity of activated carbon, and the increase in specific surface area is conducive to the increase in double electric layer capacitance in electric adsorption[14]. Fig. 4 also shows that the contribution of the two materials to pore volume is mainly mesopores, which is consistent with the above analysis. Wang et al.[15] modified activated carbon with mixed acid, which achieved a specific surface area of AC of 672.48 m²/g, i.e., an

increase of 29.43%. Jing et al.[16] modified activated carbon with KOH to have abundant mesopores and micropores, which could simultaneously improve the ion transport and charge storage.

Table 1. Specific surface area and pore structure parameters of AC before and after modification

The sample	Specific surface area (m ² /g)	Total entrance (cm ³ /g)	Average pore diameter (nm)
AC	148.17	0.16	4.3
HNO ₃ -AC	341.38	0.42	4.9

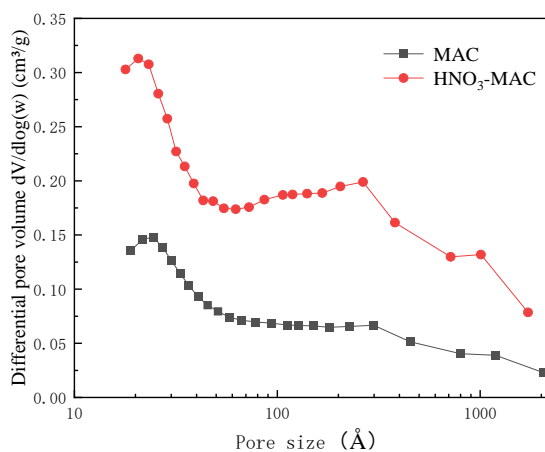


Figure 4. Pore size distribution

3.3 Raman mapping analysis

The Raman patterns of AC as-is and HNO₃-AC are shown in Figure 5.

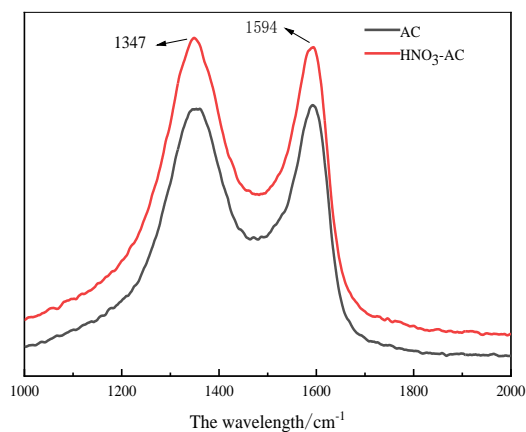


Figure 5. Raman spectra of AC before and after modification

Two characteristic peaks of AC before and after modification are shown in Fig. 5: the D-band peak at 1347 cm^{-1} represents the degree of material defects, and the G-band peak at 1594 cm^{-1} represents the degree of material graphitization[17]. After fitting the spectrum, the I_D/I_G value of AC is 0.965, while the I_D/I_G value of $\text{HNO}_3\text{-AC}$ is 1.03, which shows that the disorder degree of AC increases after modification, possibly because after the HNO_3 oxidation corrosion, the AC surface becomes rough, which increases its defect degree. The increase in defect sites is conducive to reducing material resistance, making ion transfer smoother, and consequently improving its electrical adsorption performance[18]. Grzegorz et al.[19] doped activated carbon with oxygen and found that the D/G ratio of the Raman characteristic band significantly increased, which destroyed the graphite structure of AC and reduced the resistance of the electrode material.

3.4 Infrared spectrum analysis

The FTIR spectra of the original AC and $\text{HNO}_3\text{-AC}$ are shown in Figure 6.

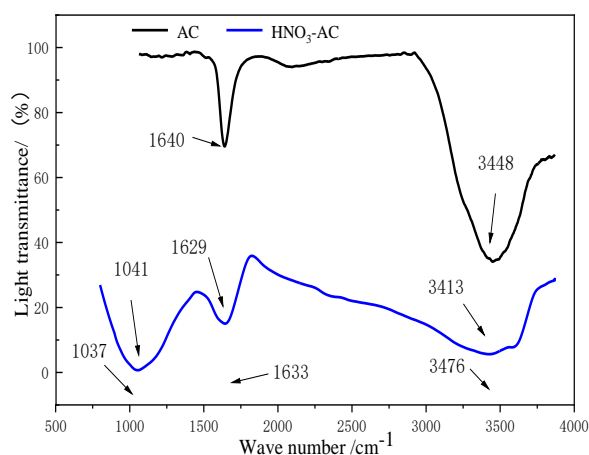


Figure 6. FTIR spectra of AC before and after modification

According to Fig. 6, the FTIR spectrum of AC before modification has two characteristic peaks corresponding to the stretching vibration peak of the $\text{C}=\text{C}$ bond at 1640 cm^{-1} and the stretching vibration peak of the $=\text{C}-\text{H}$ bond at 3448 cm^{-1} . The FTIR spectra of $\text{HNO}_3\text{-AC}$ show peaks attributed to C-H bending vibrations at 1041 cm^{-1} , $\text{C}=\text{O}$ stretching vibrations at 1629 cm^{-1} and O-H stretching vibrations at 3413 cm^{-1} , which indicates an increase in amounts of $\text{C}=\text{O}$ oxygen-containing functional groups and -O-H functional groups compared to those of unmodified activated carbon. Oxygen-containing functional groups enhance the hydrophilicity of the electrode, which makes it easier for the solution to contact the surface of the active material and facilitates ion migration during the electroadsorption process[20]. Zhao et al.[21] modified activated carbon with HNO_3 and increased its surface hydrophilic

functional groups such as carboxyl and hydroxyl groups, which enhanced the adsorption capacity of inorganic ions in solution.

3.5 XPS analysis of surface elements

Table 2 and Figure 7 show the surface chemical composition analysis results of AC before and after the HNO₃ modification by XPS.

Table 2. Surface chemical composition of AC before and after modification

No.	C1 s□	O1 s□	N1 s %
AC	69.22	14.49	1.05
HNO ₃ -AC	65.16	17.97	2.17

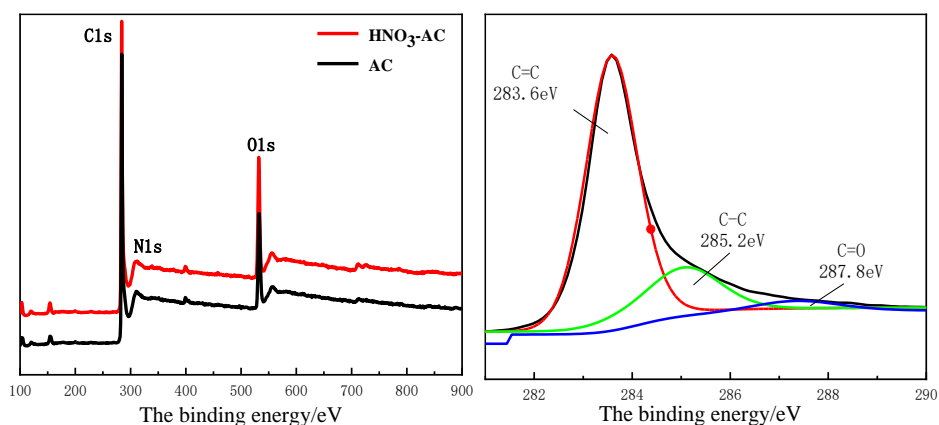


Figure 7. XPS full sweep spectrum (a) and C1s spectrum of HNO₃-AC (b)

Table 2 shows that the content of O and N elements on the AC surface after HNO₃ modification increases. According to Fig. 7 (b), AC mainly has two strong absorption peaks of C1s and O1s, which indicates that AC contains oxygen atoms on its surface. To analyze the present state of carbon elements on the surface of HNO₃-modified AC, C1s of HNO₃-AC was analyzed with high resolution. Fig. 7 (b) shows that the spectral peaks of the binding energy at 283.6, 285.2 and 287.8 eV correspond to the C=C bond, C-C bond and C=O bond, respectively[22], and new oxygen-containing functional groups appear, which is consistent with the infrared spectroscopy analysis, possibly because of the strong oxidizing property of HNO₃ and the reaction of its oxygen-containing groups with C atoms. The presence of oxygen-containing groups enhances the wettability of activated carbon and electroadsorption performance of the activated carbon electrode. Liu et al.[23] found that the surface wettability of activated carbon was enhanced by oxidative modification, which significantly improved the electrochemical properties of activated carbon, and the modified carbon increased the specific capacitance by 72.4%.

3.6 Contact angle measurement

Figure 8 shows the contact angle test of the AC electrode before modification and the HNO₃-AC/Ni electrode after modification to explore the hydrophilicity of the electrode.

The contact angle of the AC electrode before modification is 88.3° and close to 90°, which is approximately hydrophobic. The contact angle of the HNO₃-AC/Ni electrode modified by HNO₃ is 57.2°, which shows hydrophilicity. The newly introduced oxygen-containing groups (-C=O, -O-H) after modification enhance the hydrophilicity of the electrode, which indicates that the electrode is more easily infiltrated by solution, and the double electric layer formed at the interface between the electrode and the liquid phase is thickened[24], which also facilitates the diffusion process of ions from the solution to the electrode material surface. Yasin et al.[25] modified activated carbon with ZrO₂ doping, and the contact angle of the AC/ZrO₂ composite electrode decreased from 148° to 45° compared to that of the AC electrode. The modified electrode exhibited good wettability, which improved its electroadsorption capacity for salt ions.

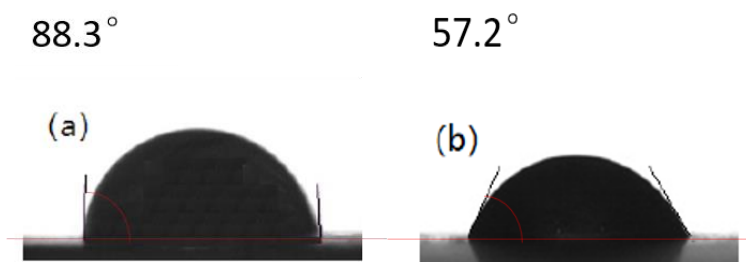


Figure 8. Contact angle of the electrode: (a) AC electrode; (b) HNO₃-AC/Ni electrode

3.7 Electrochemical performance analysis

Cyclic voltammetry tests and AC impedance tests were performed on the prepared HNO₃-AC/Ni electrode and AC electrode, respectively. The results are shown in Figure 9.

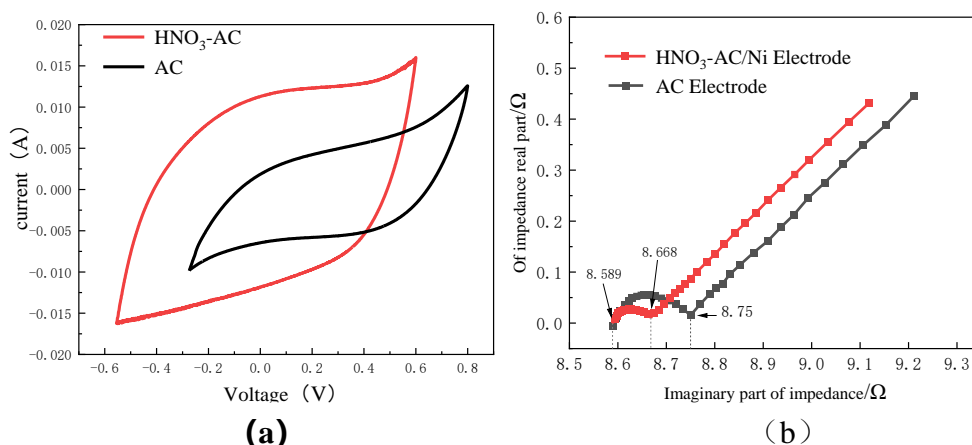


Figure 9. CV curves of the HNO₃-AC/Ni electrode measured at a scan rate of 0.05 V/s in 1 mol/L NaCl. Solution (a) and AC impedance curve (b): measured in 1 mol/L NaCl solution; frequency range: 0.001-100 kHz.

As shown in Fig. 9 (a), the cyclic voltammetry curves of the two electrodes are smooth and symmetrical, and the electrodes are sensitive to the response of the scanning voltage after its changes in magnitude and direction. There is no obvious redox peak, which indicates that the test process is a non-Faradaic process[26-27]. The specific capacitance is mainly provided by the bilayer capacitor. The cyclic voltammetry curves measured by the two electrodes are not rectangular, but the curve of the HNO₃-AC/Ni electrode is more similar to a rectangle, which indicates that in this three-electrode test system, the internal resistance of the electrode itself and internal resistance of the solution have more influence on the AC electrode and less influence on the HNO₃-AC/Ni electrode. The pore structure of AC modified by HNO₃ is more developed, and the newly added oxygen-containing functional groups make AC more hydrophilic, which results in a larger and fuller contact with the liquid phase interface of the electrolyte solution. The resistance of electrolyte ions in the mass transfer process in solution is small, which makes them more easily adsorbed on the activated carbon electrode. Thus, the desalting performance is improved.

For solid electrodes, the AC impedance curve consists of an approximately semicircular arc in the high-frequency region and an oblique line in the medium- and low-frequency regions. The two parts represent the charge transfer and diffusion processes of the electrode system, respectively[28]. The projection width of the arc in the high-frequency region represents the impedance composed of the internal resistances of the solution and electrode, which can indirectly reflect the impedance of the entire electrode[29]. As shown in Fig. 9 (b), the projection widths of the arc in the high-frequency region of the electrode before and after modification are 0.161 Ω and 0.079 Ω, respectively. The modified HNO₃-AC/Ni electrode has a lower impedance than the AC electrode, which indicates that the resistance of the charge transfer process is reduced after modification, and the electrical conductivity is good, which is conducive to the ion adsorption process and reduces the power consumption.

3.8 Adsorption characteristics of different salt ions by the HNO₃-AC/Ni electrode

3.8.1 Relation between conductivity and concentration of each ion

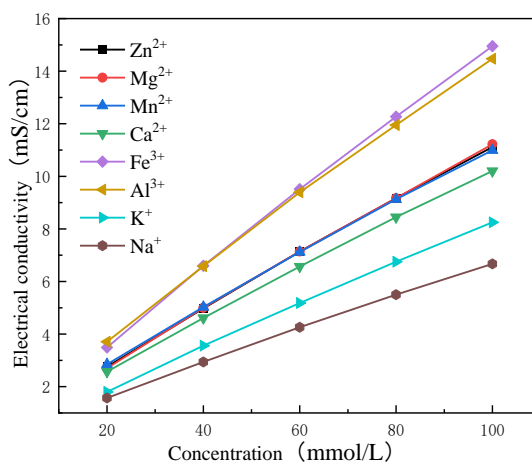


Figure 10. σ -c standard curves for different ions: the working voltage was set to 1.5 V, and the spacing between the plates was 0.5 cm.

Figure 10 shows the standard conductivity (σ)-concentration (c) curve of each ion. Table 3 shows the standard curve equations and correlation coefficients of different ions.

Table 3. Standard curve equations of different ions

Ion species	σ - c relationship equation	correlation coefficient R^2
Zn ²⁺	$\sigma = 0.1046c + 0.757$	0.9993
Mg ²⁺	$\sigma = 0.1061c + 0.683$	0.9993
Mn ²⁺	$\sigma = 0.1019c + 0.91$	0.9991
Ca ²⁺	$\sigma = 0.0955c + 0.75$	0.9991
Fe ³⁺	$\sigma = 0.143c + 0.787$	0.9991
Al ³⁺	$\sigma = 0.1345c + 1.153$	0.9991
K ⁺	$\sigma = 0.0805c + 0.281$	0.9991
Na ⁺	$\sigma = 0.0638c + 0.36$	0.9990

3.8.2 Adsorption effect of salt ions with different valence states and radii

For monovalent salt (K⁺, Na⁺), divalent salt (Ca²⁺, Mg²⁺, Zn²⁺, Mn²⁺) and trivalent salt (Al³⁺, Fe³⁺) solutions, HNO₃-AC/Ni electrodes were used for electric adsorption and desalting experiments to explore the electric adsorption properties of electrodes for different salt ions. Its adsorption effect is shown in Figure 11. The hydration ion radius, electric adsorption equilibrium time and removal rate of each ion are shown in Table 4.

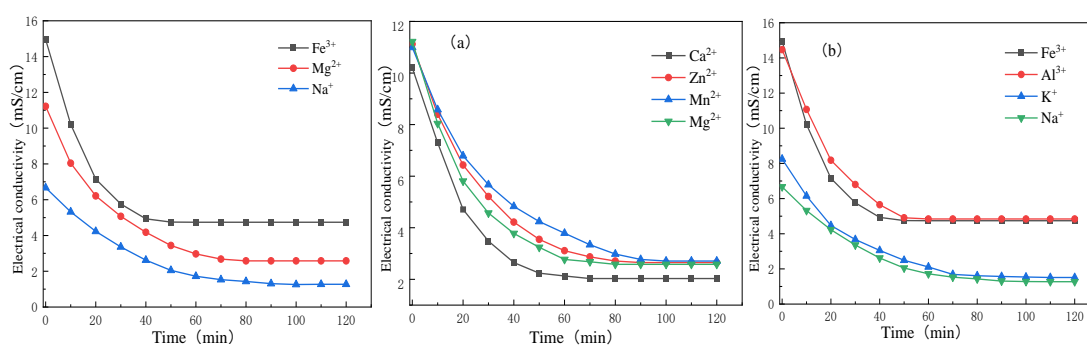


Figure 11. Adsorption effect of different ions: the working voltage was set to 1.5 V, and the spacing between the plates was 0.5 cm.

Fig. 11 (a) shows the changes in electrical conductivity of salt solutions with different valence states (represented by Na⁺, Mg²⁺ and Fe³⁺) in the electric adsorption process. A higher ionic valence state corresponds to a greater slope of the conductivity curve, i.e., a faster adsorption rate corresponds to a sooner adsorption equilibrium. However, in terms of the ion removal rate after reaching equilibrium, a higher ion valence state corresponds to a lower ion removal rate.

According to Figs. 11 (b), (c) and Table 4, the adsorption law of the electrode for homovalent ions is that a smaller ion radius requires less time to reach adsorption equilibrium, i.e., a faster adsorption rate corresponds to a higher ion removal rate and a larger adsorption capacity, since ions with smaller hydrated ion radii have less resistance to migration in the solution. Under the same electric field force, the electric adsorption process is completed faster, and the transfer is easier in the pores of electrodes and active materials. Therefore, the ions with small-radius hydrated ions have more materials adsorbed and stored in the electric double layer.

Table 4. Removal rate, adsorption equilibrium time and hydrated ion radius of each ion

Ion species	Monovalent ions			Bivalent ions			Trivalent ions	
	Na ⁺	K ⁺	Mn ²⁺	Zn ²⁺	Mg ²⁺	Ca ²⁺	Al ³⁺	Fe ³⁺
Removal rate (%)	80.86	81.7	75.34	76.17	77	80.1	66.55	68.29
Adsorption equilibrium time (min)	100	95	90	85	80	70	55	50
Radii of hydrated (nm)	0.358	0.331	0.438	0.43	0.428	0.412	0.475	0.457

Through the above analysis, it can be temporarily determined that under the experimental conditions, for ions with different valence states and different hydrated ion radii, the ion removal rates at the equilibrium of electric adsorption are in the following order: K⁺ > Na⁺ > Ca²⁺ > Mg²⁺ > Zn²⁺ > Mn²⁺ > Fe³⁺ > Al³⁺.

3.9 Adsorption kinetics analysis

3.9.1 Quasi-first-order adsorption kinetics analysis

Different adsorption kinetics models were used to fit the adsorption data of each ion. According to Equations (1), (2) and (4) in Table 3, the relationship between the adsorption capacity and the electric adsorption reaction time was calculated, and the quasi-first-order reaction kinetic model was fitted to obtain the first-order reaction rate constant and equilibrium adsorption capacity. The fitting effect is shown in Figure 12, and the fitting parameters are shown in Table 5.

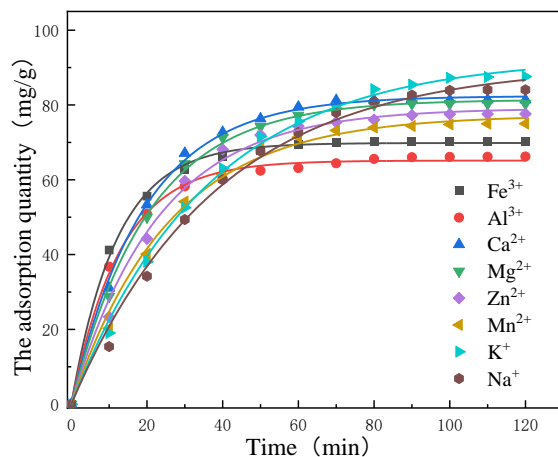


Figure 12. Quasi-first-order adsorption model fitting for different ions: the working voltage was set to 1.5 V, and the spacing between the plates was 0.5 cm.

The R^2 value in Table 5 shows that the fitting degree is above 0.99, which indicates a high fitting degree. The electrical adsorption process conforms to the quasi-first-order adsorption kinetic model, which is mainly a physical adsorption process. Fig. 12 shows that the adsorption of each ion rapidly increases in the first 20 min because in the early stage of adsorption, the external diffusion process from the solution to the electrode surface is relatively fast. At 20-40 min, the growth rate of the adsorption capacity obviously decreases and subsequently gradually reaches equilibrium. A comparison of the equilibrium adsorption quantity q_e and adsorption rate constant k_1 in Table 5 shows that in the electric adsorption process, a higher valence state of the ion corresponds to faster adsorption, and a smaller radius of the hydrated ion in the same valence state corresponds to a larger adsorption capacity. From the adsorption rate constant of each ion, the adsorption rates of ions of the same valence do not differ much; however, the adsorption rates of ions of different valences significantly differ. The ion valence has a large influence on the electrosorption process, which is shown by the trend of the fitted curve in Fig. 12 and is consistent with the results of the above analysis.

Table 5. Quasi-first-order adsorption model fitting parameters for different ions

Ion species	q_e (mg/g)	k_1 (min^{-1})	R^2
Fe^{3+}	69.84203	0.08277	0.99792
Al^{3+}	65.14445	0.07696	0.99598
Ca^{2+}	82.3935	0.05238	0.9981
Mg^{2+}	81.41524	0.04876	0.99792
Zn^{2+}	79.13729	0.04362	0.99351
Mn^{2+}	77.26577	0.03864	0.99389
K^+	92.71654	0.02779	0.99718
Na^+	90.71137	0.02605	0.99354

3.9.2 Quasi-second-order adsorption kinetics analysis

Based on Equations (1), (2) and (5), the relational equations in Table 3, a quasi-secondary reaction kinetic model was fitted to obtain their second-order reaction rate constants and equilibrium adsorption quantity, which are shown in Fig. 13. The fitting parameters are shown in Table 6.

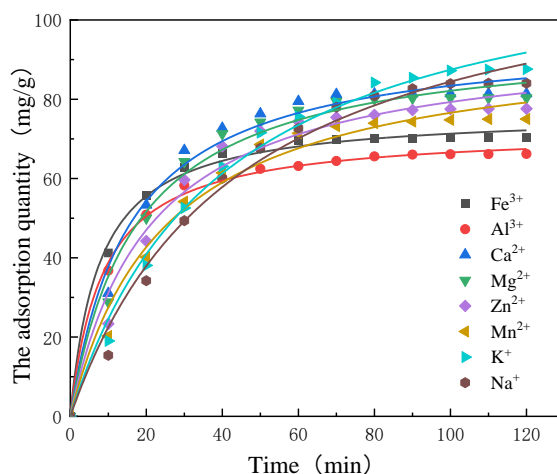


Figure 13. Quasi-secondary adsorption model fitting for different ions: the working voltage was set to 1.5 V, and the spacing between the plates was 0.5 cm.

Table 6. Fitting parameters of the quasi-secondary adsorption model for different ions

Ion species	q_e (mg/g)	k_2 (min^{-1})	R^2
Fe^{3+}	76.74263	0.00171	0.99503
Al^{3+}	72.30318	0.00160	0.99679
Ca^{2+}	96.3138	0.00007	0.98231
Mg^{2+}	96.30625	0.00060	0.98293
Zn^{2+}	95.72711	0.00050	0.97558
Mn^{2+}	95.52012	0.00042	0.97795
K^+	122.19321	0.00021	0.98011
Na^+	121.75304	0.00019	0.98467

The fitting parameter R^2 of the adsorption model in Fig. 13 and Table 6 shows that the fit of quasi-secondary adsorption for this electrosorption process is worse than that of the quasi-primary adsorption model. However, all fitting parameters for the adsorption of trivalent ions Fe^{3+} and Al^{3+} were above 0.99, which is consistent with the quasi-second-order adsorption model. The theoretical equilibrium adsorption capacity increased, which indicates that chemical adsorption occurred in the adsorption process. The reason is that the modified HNO_3 -AC active material has more oxygen-

containing functional groups on its surface, which act as electron-absorbing groups to provide more adsorption sites for this adsorption process. Electron sharing may occur with trivalent ions of higher charge. This process is often slow.

3.9.3 Intraparticle diffusion analysis

According to Equations (1), (2) and (6), the relational equations in Table 3, the intraparticle diffusion model fitting was performed to obtain its reaction rate constants, which are shown in Figure 14. The fitting parameters are shown in Table 7.

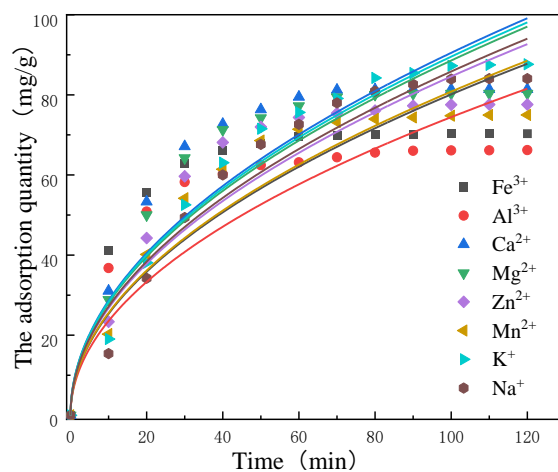


Figure 14. Intraparticle diffusion model for different ions: the working voltage was set to 1.5 V; the spacing between the plates was 0.5 cm.

Table 7. Parameters for the intraparticle diffusion model fitting for different ions

Ion species	K_n (min^{-1})	r^2
Fe^{3+}	8.01149	0.46896
Al^{3+}	7.44364	0.40818
Ca^{2+}	9.04892	0.41207
Mg^{2+}	8.8568	0.37921
Zn^{2+}	8.45852	0.34302
Mn^{2+}	8.07978	0.29454
K^+	8.95356	0.21725
Na^+	8.58248	0.22528

Obviously, Fig. 14 and Table 7 show that the fit of the intraparticle diffusion of this electrosorption process is extremely poor. Poor applicability is also observed from parameter r^2 . This

process does not conform to the intraparticle diffusion process and does not involve chemical reactions on the internal micropores of the particles.

4. CONCLUSION

(1) HNO₃-AC has better pore structure, specific surface area and electrochemical performance than AC before modification. After modification, C=O and -O-H oxygen-containing functional groups are added, which improves the hydrophilicity of the HNO₃-AC/Ni electrode.

(2) The adsorption of eight salt ions by the HNO₃-AC/Ni electrode shows the following adsorption characteristics: a higher valence state corresponds to a faster adsorption rate and a smaller equilibrium adsorption capacity. In the same valence state, a smaller radius of the hydrated ion corresponds to a faster adsorption rate and a larger equilibrium adsorption capacity. The adsorption rates of the eight ions in descending order are Fe³⁺ > Al³⁺ > Ca²⁺ > Mg²⁺ > Zn²⁺ > Mn²⁺ > K⁺ > Na⁺. The equilibrium adsorption capacity in descending order is K⁺ > Na⁺ > Ca²⁺ > Mg²⁺ > Zn²⁺ > Mn²⁺ > Fe³⁺ > Al³⁺.

(3) The electric adsorption process of univalent and divalent ions is more consistent with the quasi-first-order adsorption model and mainly a physical adsorption process. The quasi-second-order adsorption model is more suitable for trivalent ions, which indicates that the process from solution to the electrode surface and subsequently to the pore of the active material has a physical adsorption process and a slower chemical adsorption process.

ACKNOWLEDGMENTS

This work was financially supported by the National Natural Science Fund of China (No. 42007415) and the Natural Science Foundation of Shaanxi Province (No. 2020SF-435).

References

1. B. B. Arnold, G.W. Murphy, *J. Phys. Chem. A.*, 65 (1961) 135.
2. M. Macher, S. Hassan, K. Shoueir, B. Yousif, M. Eldin and A. Elsoudg, *J. Mater. Res. Technol.*, 11 (2021) 1232.
3. G. Folaranmi, M.B. Echelany, P. Sstat, M. Cretin and F. Zaviska, *Materials*, 13 (2020) 5185.
4. Q.H. Wu, D.W. Liang, E. Avraham, *Desalination*, 491 (2020) 114460.
5. T. Alencherry, A.R. Nav, S. Ghosh, J. Daniel et al., *Desalination*, 415 (2017) 14.
6. L. Zou, G. Morris, D. Qi, *Desalination*, 225 (2008) 329.
7. Z.L. Chen, C.Y. Song, X.W. Sun, H.F. Guo and G.D. Zhu, *Desalination*, 267 (2011) 239.
8. C. Moreno-castilla, F. Carrasco-marín, F.J. Maldonado-hódar, J. Rivera-utrilla, *Carbon*, 36 (1998) 145.
9. C.H. Hou, J.F. Huang, H.R. Lin, *J. Taiwan Inst. Chem. Eng.*, 43 (2012) 473.
10. H. Liu, H. Li, K. Yang, *Int. J. Electrochem.*, 15 (2020) 6122.
11. S. Jiang, H. Wang, G. Xiong, *Water Supply*, 18 (2018) 2028.
12. K.S. Walton, R.Q. Snurr, *J. Am. Chem. Soc.*, 129 (2007) 8552.
13. C.S. Katie, T. Matthias, S. Lev, *Adv. Mater. Interfaces*, 7 (2020) 2000184.

14. G. Wang, B. Qian, Q. Dong, *Sep. Purif. Technol.*, 103 (2013) 216.
15. L. Wang, S.H. Yu, L.F. Yi, *Water Supply*, 19 (2019) 2054.
16. J. Sun, S.H. Yang, S.S. Li, *Rare Met.*, 36 (2017) 449.
17. Y. Cao, K. Han, Z. Teng, *J. Alloys Compd.*, 860 (2021) 158385.
18. R. Santhosh, S.R.S. Raman, S.M. Krishna, *Electrochim. Acta*, 276 (2018) 284.
19. G. Milczarek, A. Ciszewski, I. Stepniak, *J. Power Sources*, 196 (2011) 7882.
20. D.W. Wang, L.I. Feng, L.I.U. Min, *New Carbon Mater.*, 22 (2007) 307-314.
21. Z.L. Chen, X.W. Sun, H.F. Guo, *Adv Mat Res.*, 113 (2010) 2134.
22. Q. Fang, X. Zhou, W. Deng, *Small*, 13 (2017) 1603779.
23. Y. Liu, Z. Hu, K. Xu, *Acta Phys. Chim. Sin.*, 24 (2008) 1143.
24. P. Justin, S.K. Meher, G.R. Rao, *J. Phys. Chem. C.*, 114 (2010) 5203.
25. A.S. Yasin, I.M.A. Mohamed, M.T. Amen, *J. Alloys Compd.*, 772 (2019) 1079.
26. P. Setiarso, P. Sari, *Asian J. Chem.*, 33 (2021) 757.
27. S. Wadhav, Y. Jadhav, P. Thakur, *Sol. Energy Mater. Sol. Cells.*, 223 (2021) 110958.
28. Z. Siroma, T. Sato, T. Takeuchi, *J. Power Sources*, 316 (2016) 215.
29. A. Kilic, D. Eroglu. *Chemelectrochem*, 8 (2021) 963.

© 2022 The Authors. Published by ESG (www.electrochemsci.org). This article is an open access article distributed under the terms and conditions of the Creative Commons Attribution license (<http://creativecommons.org/licenses/by/4.0/>).